Supporting Information

Haudin et al. 10.1073/pnas.1409552111

SI Text

Geometrical Model: Alternative Derivation

Intrinsic Equation. We give here an alternative and equivalent derivation of the equation describing the curve generated by the geometrical model. This derivation is independent of the coordinate system and leads to a so-called natural (or intrinsic) equation giving the evolution of the local radius of curvature of the curve as a function of the arclength (ref. 1, p. 26).

We still consider the system at two infinitesimally close time steps such that the length of the curve has increased by an amount ds given by Eq. **1** of the main text, namely

$$ds = \theta_0\, dr_b = \theta_0 \frac{dr_b}{dt} dt, \qquad \text{[S1]}$$

where $r_b(t)$ is the radius of the bubble of injected reagent at time t (Fig. S1*A*). The curve is parametrized by its arclength s such that the value of s of an arbitrary point P is equal to the length of the curve measured from the first point P_0 to P (Fig. S1*A*). As explained in the main text, P_0 is generated from an initial small circle of radius $r_b(0) = r_c$. The radius of curvature at $s = 0$ is thus given by $R(0) = r_c$. At time t, the radius of curvature of the last point of the curve at its tail is given by

$$R(s) = r_b(t). \qquad \text{[S2]}$$

Similarly, at time $t + dt$, the radius of curvature of the last point of the curve is given by

$$R(s + ds) = r_b(t + dt) = r_b(t) + \frac{dr_b}{dt} dt, \qquad \text{[S3]}$$

where we used a first-order expansion in dt. Therefore, the difference between Eq. **S3** and Eq. **S2** leads to

$$R(s + ds) - R(s) = \frac{dR}{ds} ds = \frac{dr_b}{dt} dt, \qquad \text{[S4]}$$

where we used a first-order expansion in ds. Using the expression **S1** of ds, we obtain

$$\frac{dR}{ds} = \frac{1}{\theta_0}. \qquad \text{[S5]}$$

Integration of this last equation leads to

$$R(s) = R(0) + \frac{s}{\theta_0} = r_c + \frac{s}{\theta_0}. \qquad \text{[S6]}$$

The radius of curvature is thus a linear function of the arclength. This is the Cesàro equation of a logarithmic (equiangular) spiral (ref. 1, p. 26). Let us now obtain the equation of the curve in polar coordinates.

Polar Equation. We have thus obtained above the curvature κ as a function of the arclength s:

$$\kappa(s) = \frac{1}{R(s)} = \frac{\theta_0}{\theta_0 r_c + s}. \qquad \text{[S7]}$$

The relation between the Cesàro equation and the Cartesian coordinates is (ref. 1, p. 26)

$$x(s) = \int \cos\overline{\kappa}(s) ds = \frac{\theta_0 r_c + s}{1 + \theta_0^2} (\cos\overline{\kappa}(s) + \theta_0 \sin\overline{\kappa}(s)), \qquad \text{[S8a]}$$

$$y(s) = \int \sin\overline{\kappa}(s) ds = \frac{\theta_0 r_c + s}{1 + \theta_0^2} (\sin\overline{\kappa}(s) - \theta_0 \cos\overline{\kappa}(s)), \qquad \text{[S8b]}$$

where

$$\overline{\kappa}(s) = \int \kappa(s) ds = \theta_0 \ln(\theta_0 r_c + s) + K, \qquad \text{[S9]}$$

and K is a constant of integration which fixes the orientation of the curve in space and is fixed below. The constants of integration in Eq. **S8** correspond to translations of the curve and are set to zero.

Using Eqs. **S8** and **S9**, the polar equation is obtained as follows:

$$r(s) = \sqrt{x^2(s) + y^2(s)} = \frac{\theta_0 r_c + s}{\sqrt{1 + \theta_0^2}}, \qquad \text{[S10]}$$

and

$$\begin{aligned} \theta(s) &= \arctan\left(\frac{y}{x}\right) = \arctan\left(\frac{\sin\overline{\kappa}(s) - \theta_0 \cos\overline{\kappa}(s)}{\cos\overline{\kappa}(s) + \theta_0 \sin\overline{\kappa}(s)}\right) \\ &= \arctan\left(\frac{\tan\overline{\kappa}(s) - \theta_0}{1 + \theta_0 \tan\overline{\kappa}(s)}\right) \\ &= \arctan[\tan(\overline{\kappa}(s) - \arctan\theta_0)] \\ &= \overline{\kappa}(s) - \arctan\theta_0 \\ &= \theta_0 \ln(\theta_0 r_c + s) + K - \arctan\theta_0. \end{aligned} \qquad \text{[S11]}$$

Eliminating s between Eqs. **S10** and **S11**, we have

$$r = \frac{e^{(\arctan\theta_0 - K)/\theta_0}}{\sqrt{1 + \theta_0^2}} e^{\theta/\theta_0}. \qquad \text{[S12]}$$

The constant K can be fixed by imposing that $s = 0$ corresponds to $\theta = 0$, meaning that the radius of curvature of the curve **S12** at $\theta = 0$ should be equal to r_c. This leads to $K = \arctan\theta_0 - \theta_0 \ln(\theta_0 r_c)$ and Eq. **S12** reduces to

$$r = \frac{r_c \theta_0}{\sqrt{1 + \theta_0^2}} e^{\theta/\theta_0} \equiv r_0\, e^{\theta/\theta_0}. \qquad \text{[S13]}$$

Discrete Algorithm

The curves generated by the proposed mechanism and depicted schematically in Fig. S1*A* can also be directly constructed using the following discrete algorithm (Fig. S1*B*). We start from a circle of radius r_c with a point P_0 at the top which represents the first point of the generated curve.

i) The radius of the circle is increased by a given Δr. The ordinate of P_0 is increased by Δr and then rotated by an angle $\Delta\theta$. A point P_1 is added at the top of the circle and represents a new amount of precipitate.

ii) The radius of the circle is increased by a constant Δr. The ordinates of P_0 and P_1 are increased by Δr and then are both rotated by an angle $\Delta\theta$. A point P_2 is added at the top of the circle.

The procedure is then iterated to generate the next points. The discrete angle used is provided by Eq. **3** of the main text: $\Delta\theta = \theta_0 \Delta r/r$. Fig. S1*B* shows the generation of the first few points using a large value of Δr for clarity. Fig. S1*C* shows the resulting structures emerging from the 2,000 and 4,000 iterations of the algorithm using a smaller value of $\Delta r = 0.01$ and $\theta_0 = 2$. Fig. S1*D* shows that these two curves, once properly rotated and translated, are exactly described by Eq. **S13** using the same value of θ_0 as the one used in the algorithm and a value of r_0 such that the radius of curvature at P_0 is equal to the radius r_c of the initial small circle, namely $r_0 = r_c\theta_0/(1+\theta_0^2)^{1/2}$.

Spiral Analysis

Each experiment is recorded by taking photos at regular time steps adapted according to the injection rate. Typically the time interval between two photos is 1 s for the injection rates used. The pattern is then analyzed at one given time for each experiment when the spirals are sufficiently developed and/or when the overall pattern is as large as the field of view. To analyze the spirals observed in our experiments, we measure the evolution of the spiral radii r as a function of the polar angle θ. By convention, the starting point P_0 of the spiral, which is the closest to the spiral center, is characterized by $\theta = 0$ and $r = r_0$ (Fig. S2). However, the exact position of the spiral center C_S, from which the radii should ideally be measured, is not known. In this section, we explain the method used to overcome this difficulty.

System of Coordinates Centered on the Spiral Center. The equation of a logarithmic spiral written in a system of coordinates centered on the spiral center C_S is given by

$$r = r_0 e^{\theta/\theta_0}, \qquad \textbf{[S14]}$$

where r_0 and θ_0 are constant parameters. If the spiral radii r are measured from the exact position of the spiral center C_S, then the evolution of r as a function of the polar angle θ can be fitted using Eq. **S14**. The measured spiral radii and the polar angle can then be rescaled by r_0 and θ_0, respectively, to produce the graph displayed in Fig. 3*B* of the main text.

Arbitrary System of Coordinates. The exact position of the spiral center is generally not known a priori and the radii are measured in an arbitrary system of coordinates whose origin does not coincide with C_S. In such a system of coordinates centered on, say, C_A, the expression of a logarithmic spiral is no longer given by the simple form Eq. **S14**. In this section, we derive the general expression describing a logarithmic spiral off centered with regard to C_S which is used to fit the data.

The approximate position of the spiral center C_A used to measure the spiral radii is obtained from the osculating circle passing through P_0. Fig. S2*A* shows this construction on an exact logarithmic spiral to illustrate and test the proposed procedure. Fig. S2*B* shows the evolution of the spiral radii r as a function of the polar angle θ when the radii are measured from the exact (C_S) and approximate (C_A) positions of the spiral center, respectively. The polar coordinates of the spiral obtained from the approximate position of the center are noted (r', θ'), whereas the polar coordinates of the spiral obtained from the exact position of the center are noted (r, θ).

These two curves are obviously equivalent and describe the same spiral. As shown in Fig. S3, they are just measured in two different systems of coordinates related by a rotation and a translation as

$$\begin{pmatrix} x \\ y \end{pmatrix} = \begin{pmatrix} \cos\varphi & -\sin\varphi \\ \sin\varphi & \cos\varphi \end{pmatrix} \begin{pmatrix} x' \\ y' \end{pmatrix} - \begin{pmatrix} x_0 \\ y_0 \end{pmatrix}, \qquad \textbf{[S15]}$$

with

$$\varphi = \arcsin\left(\frac{y_0}{r_0'}\right), \quad x' = r'\cos\theta', \quad y' = r'\sin\theta'. \qquad \textbf{[S16]}$$

x_0 and y_0 are the Cartesian coordinates of C_A in the (x,y) system of coordinates whose origin coincides with the spiral center C_S. Because r', θ', and r_0' are the quantities measured in practice, the curve (r,θ) obtained from the exact position of the center can thus be reconstructed once x_0 and y_0 are known by using

$$r = \sqrt{x^2+y^2}, \quad \theta = \arccos\left(\frac{x}{r}\right). \qquad \textbf{[S17]}$$

Notice that if the spiral is exactly logarithmic and if the approximate center is constructed using the osculating circle passing through P_0, then $x_0 = 0$ as seen in Fig. S2*A*. In practice, the spirals are obviously never exactly logarithmic and the position of the osculating circle is never perfect. Consequently, one needs to allow for a nonvanishing value for x_0 in the procedure. We show below how x_0 and y_0 can be obtained.

The spiral parameters r_0 and θ_0, together with the translation parameters of the center x_0 and y_0, are obtained all at once by fitting the data by the general expression of a logarithmic spiral valid in an arbitrary system of coordinates. This general expression is simply obtained by considering the reverse of the transformation **S15**:

$$\begin{pmatrix} x' \\ y' \end{pmatrix} = \begin{pmatrix} \cos\varphi & \sin\varphi \\ -\sin\varphi & \cos\varphi \end{pmatrix} \begin{pmatrix} x+x_0 \\ y+y_0 \end{pmatrix}, \qquad \textbf{[S18]}$$

with

$$x = r_0 e^{t/\theta_0}\cos t, \quad y = r_0 e^{t/\theta_0}\sin t, \qquad \textbf{[S19]}$$

and φ is given by Eq. **S16**. The parametric equations, where t is the parameter describing a logarithmic spiral in an arbitrary system of coordinates, are finally given by

$$r'(r_0,\theta_0,x_0,y_0;t) = \sqrt{x'^2+y'^2}, \qquad \textbf{[S20a]}$$

$$\theta'(r_0,\theta_0,x_0,y_0;t) = \arccos\left(\frac{x'}{r'}\right). \qquad \textbf{[S20b]}$$

The values of the parameters r_0, θ_0, x_0, and y_0 are obtained for each spiral by fitting the expression **S20** to the measured values of r' and θ' using a nonlinear regression procedure (Mathematica).

At this stage, because x_0 and y_0 are known, we apply the transformation **S15** to the data to obtain the measured curve in a system of coordinates centered on the spiral center. The result is shown in Fig. S2*B* with a very good agreement compared with the measurements performed directly in a system of coordinates centered on the spiral center. This illustrates the correctness of the procedure proposed to treat the data.

Results from the Analysis

The results of the analysis described in the previous section are gathered in Fig. 3*B* of the main text where the radial distance and the polar angle are rescaled by r_0 and θ_0. The same results are presented here separately for each categories S_i defined in Fig. 1 of the main text. The spirals are logarithmic in good approximation in each of the seven sectors S_i of the phase diagram (Fig. S4 below).

Only the sector S_1 displays more dispersion for low values of θ/θ_0 but, at larger values of the rescaled polar angle, the spirals follow closely the evolution of a logarithmic spiral. For information, we also show in Fig. S4*H* the results obtained for the inverted case, where sodium silicate is injected into cobalt chloride, corresponding to the sectors S_1 and S_3. Those spirals are also logarithmic.

In Fig. S5, we show the distributions of the values of r_0 and θ_0 characterizing all of the analyzed spirals. Those distributions show also the contributions of each sector S_i. Notice that those distributions have a meaning only if r_0 and θ_0 are both independent of the reagent concentrations (or if the dependence is weak). It seems that this is roughly the case by inspecting the contributions of each sector S_i. However, the number of analyzed spirals per sector is not large enough to draw definitive conclusions. Notice that the sector S_2 is characterized by larger values of r_0 ($r_0 \gtrsim 0.5$ mm). However, only seven spirals have been analyzed for this sector. For clarity, those data are not reported in Fig. S5*A*. The distributions of r_0 and θ_0 are both rather well fitted by a log-normal distribution

$$f(x;\mu,s) = \frac{\lambda}{x} e^{-\left[(\ln x-\mu)^2/2s^2\right]}. \quad \textbf{[S21]}$$

The expectation value E is then given by

$$E = e^{\mu+s^2/2}, \quad \textbf{[S22]}$$

and the SD σ is

$$\sigma = \left(e^{s^2}-1\right)^{1/2} E. \quad \textbf{[S23]}$$

We find

$$r_0 = (0.43 \pm 0.20)\text{mm}, \quad \theta_0 = 1.67 \pm 0.52. \quad \textbf{[S24]}$$

1. Struik DJ (1988) *Lectures on Classical Differential Geometry* (Dover Publications, New York), 2nd Ed.

Within our minimal geometric model, the radius of curvature of the spiral at its starting point P_0 should be close to the radius r_c of the initial circle of solid precipitate before the solid layer breaks. The radius of curvature R of a logarithmic spiral is given by

$$R = r_0\, e^{\theta/\theta_0} \frac{\sqrt{1+\theta_0^2}}{\theta_0}. \quad \textbf{[S25]}$$

Consequently, at the point P_0 ($\theta = 0$), the radius of curvature $R_{P_0} \equiv r_c$ is given by

$$r_c = r_0 \frac{\sqrt{1+\theta_0^2}}{\theta_0}. \quad \textbf{[S26]}$$

The distribution of r_c in the experiments is displayed in Fig. S6*A* and also follows a log-normal distribution. We find

$$r_c = (0.51 \pm 0.24)\text{mm}. \quad \textbf{[S27]}$$

Three typical spirals constructed by considering a constant value of r_c equal to its expectation value and θ_0 varying by 1 SD around its expectation value are shown in Fig. S6*B*. Those three spirals are generated from the same expanding bubble of reagent having a radius equal to 40 r_c. Consequently, they all have the same pair of radii of curvature at their end points. An animation showing the growth of these spirals can be found in Movie S2. Movie S3 shows a qualitative comparison between the growth a spiral observed experimentally and a spiral obtained from the geometrical model.

Finally, Fig. S7 shows the distribution of the maximal value θ_{max} of the polar angle characterizing each analyzed spiral. As explained in the main text, we choose $\theta_{max} > 2.44$ (140°) such that the maximal value of θ/θ_0 for each spiral is large enough to obtain a relevant comparison with the model.

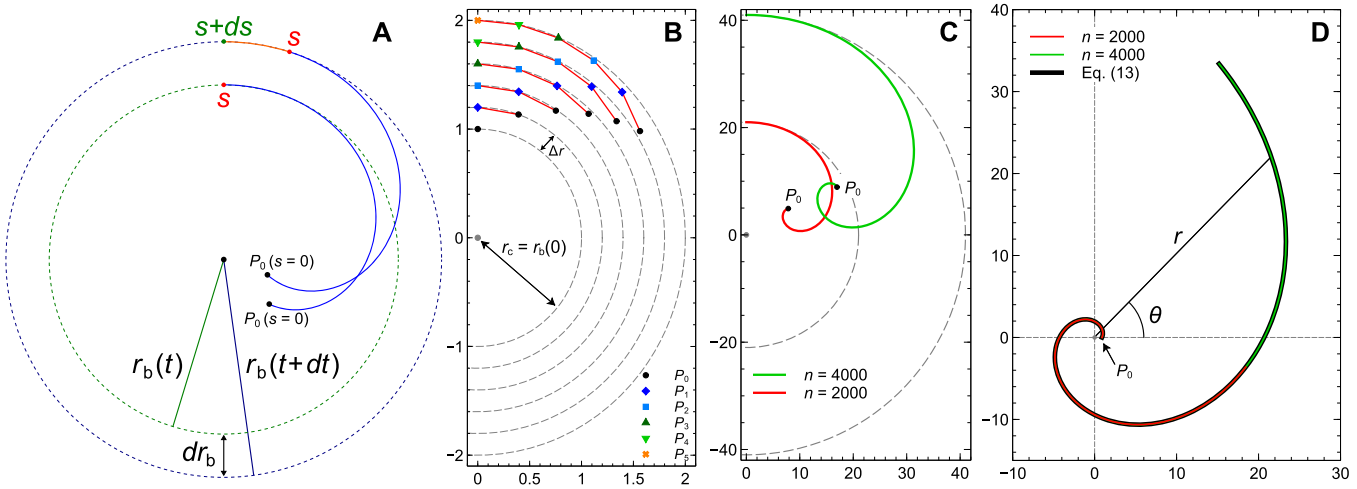

Fig. S1. (*A*) Schematic of the growth mechanism of the curly shaped precipitates during an infinitesimal interval of time. (*B*) First few points generated by this mechanism and obtained from a discrete algorithm using $\Delta r = 0.2$, $\theta_0 = 2$, and $r_c = 1$. The red straight lines are added to help with visualizing the emerging structure. Due to symmetry, the generation of only one curve is shown. (*C*) Curves generated from a discrete algorithm using $\Delta r = 0.01$, $\theta_0 = 2$, and $r_c = 1$. The curves obtained after $n = 2{,}000$ and $n = 4{,}000$ iterations are shown and correspond to a bubble of injected reagent having a radius of $21r_c$ and $41r_c$, respectively ($n\Delta r + r_c$). (*D*) If the emerging curves are logarithmic spirals, the position of the spiral center can be deduced from the position of the center of curvature of P_0 (see *Spiral Analysis*). In the context of this algorithm, the position of the center of curvature of P_0 is tracked during the growth process. The total angle of rotation of the curves during the growth is simply equal to the sum of all $\Delta\theta$ applied. Therefore, these two curves can be properly rotated and translated such that their centers coincide with the origin of coordinates. These curves are exactly described by Eq. **S13** with $\theta_0 = 2$ and $r_0 = r_c\theta_0/(1+\theta_0^2)^{1/2} \simeq 0.89$, such as its radius of curvature at P_0 ($\theta = 0$) is equal to r_c.

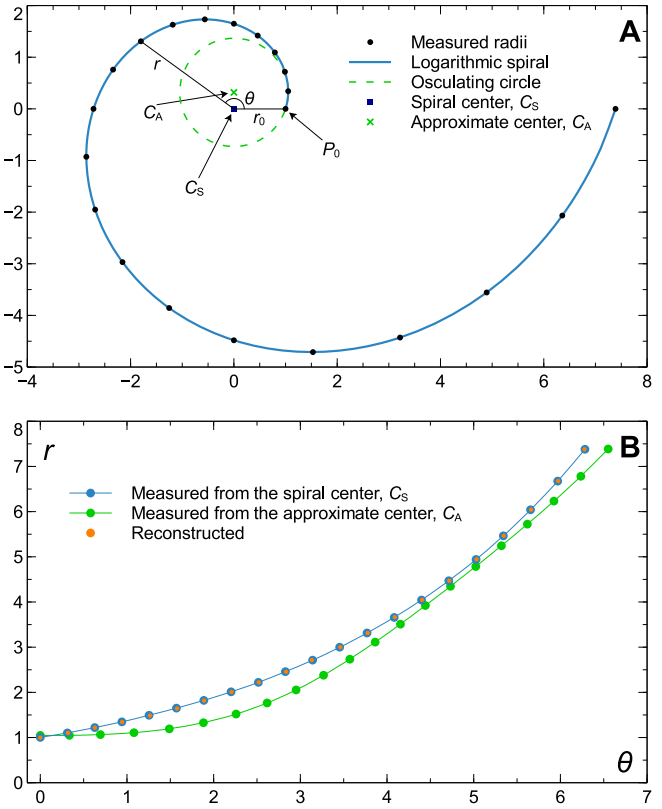

Fig. S2. (*A*) Logarithmic spiral together with the osculating circle passing through the point P_0 which is the closest to the spiral center. The center of the osculating circle C_A is used as approximate center to measure the spiral radii. The black dots show where the radii are measured. C_S indicates the position of the spiral center. (*B*) Plot of the radius r of the spiral as a function of the polar angle θ using the exact and the approximate positions of the spiral center. The curve reconstructed from the data obtained with the approximate position of the spiral center is also shown (orange dots) and agrees well with the spiral curve measured directly from the exact center position C_S.

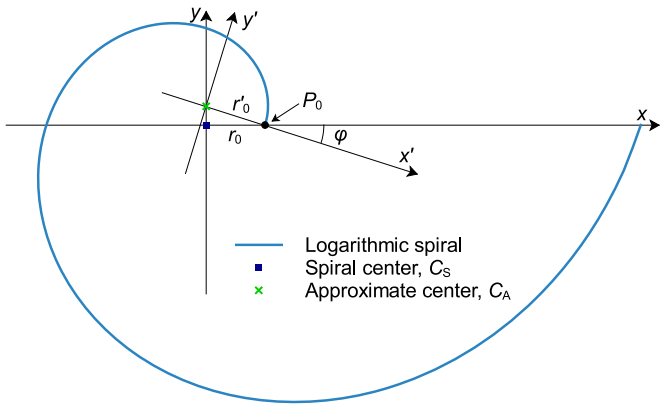

Fig. S3. Representation of the two systems of coordinates. The system of coordinates (x,y) is centered on the spiral center C_S, whereas the system of coordinates (x',y') is centered on C_A and is used to measure the spiral radii.

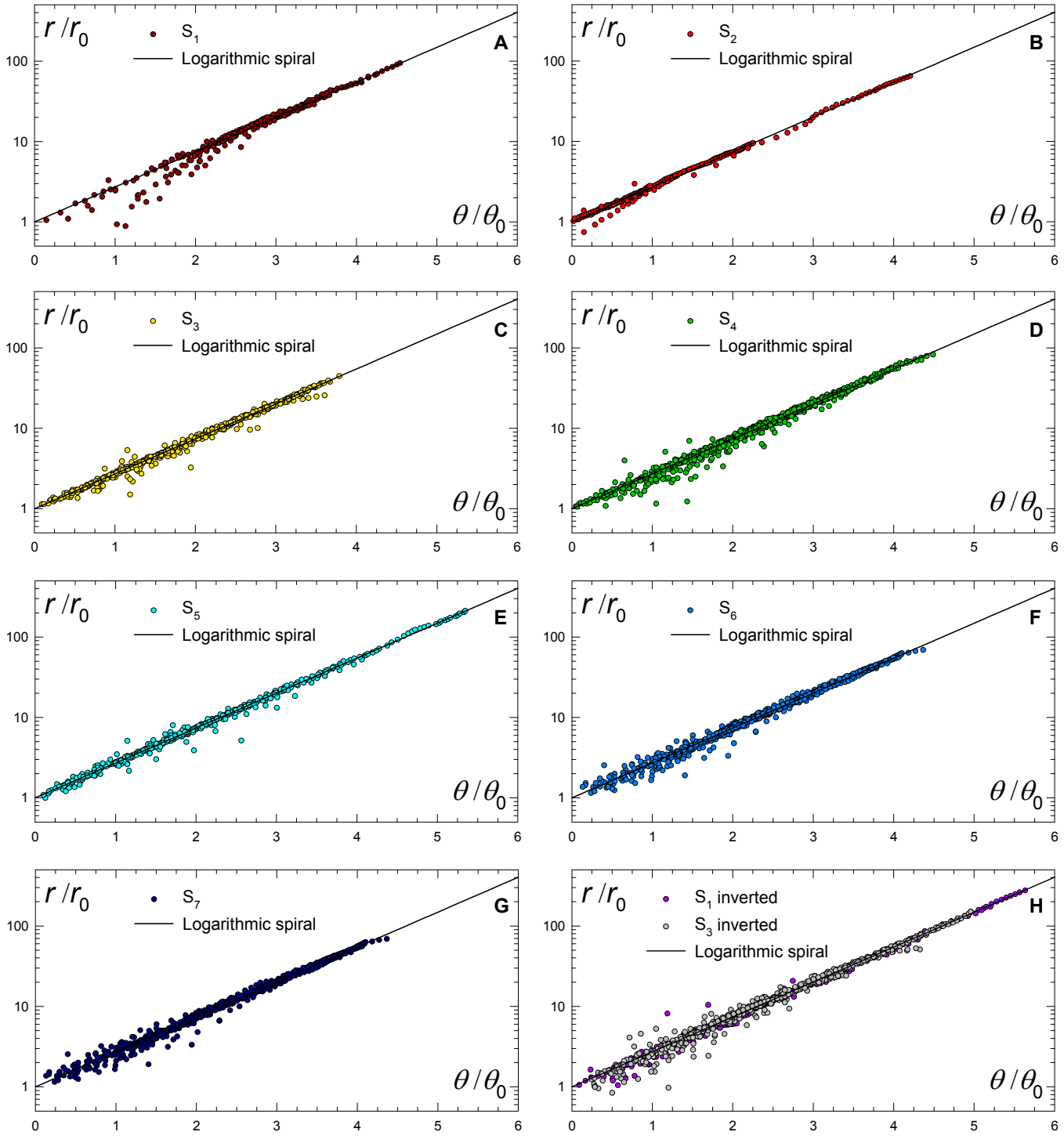

Fig. S4. (*A*–*G*) Evolution of the rescaled spiral radii r/r_0 as a function of the rescaled polar angle θ/θ_0 for each category S_i identified in Fig.1 of the main text. (*H*) Evolution of the rescaled spiral radii r/r_0 as a function of the rescaled polar angle θ/θ_0 for the inverted case, where sodium silicate is injected into cobalt chloride, corresponding to the sectors S_1 and S_3.

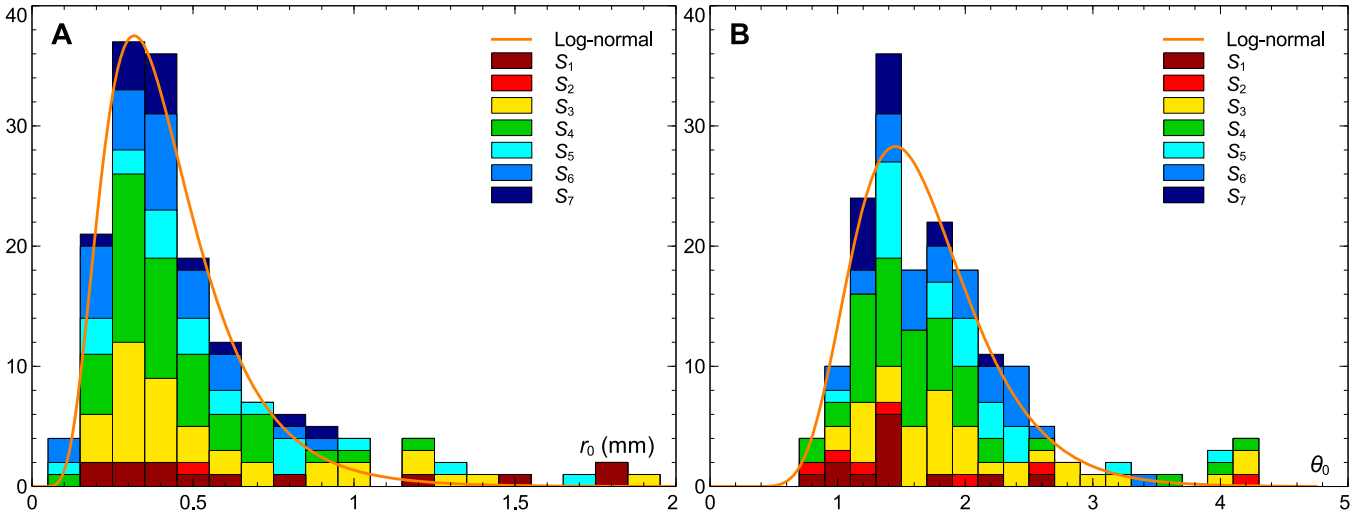

Fig. S5. (*A*) Distribution of r_0 and (*B*) distribution of θ_0 for all analyzed spirals. The contributions of each sector S_i are indicated. The log-normal distributions **S21** are characterized by $\mu = -0.97$ and $s = 0.45$ for r_0 and $\mu = 0.47$ and $s = 0.31$ for θ_0.

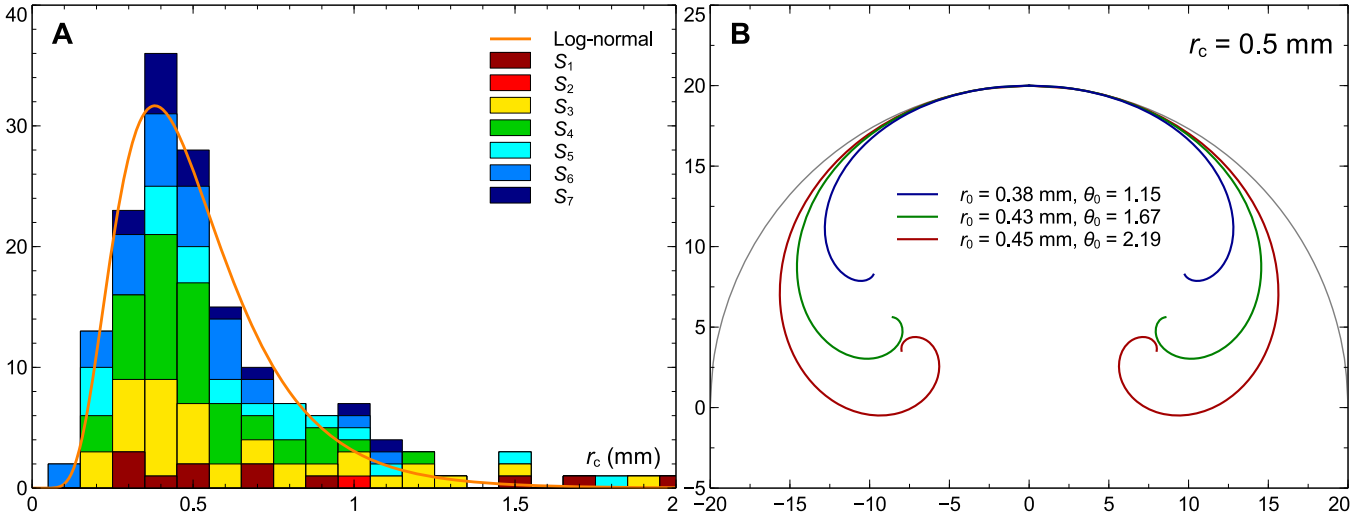

Fig. S6. (*A*) Distributions of r_c for all analyzed spirals. The contribution of each sector S_i is indicated. The log-normal distribution **S21** is characterized by $\mu = -0.77$ and $s = 0.47$. (*B*) Three typical spirals constructed by considering a constant value of r_c equal to its expectation value and θ_0 varying by 1 SD around its expectation value. The spirals are generated from the same expanding bubble (in gray) of reagent having a radius equals to 40 r_c. Consequently, they all have the same pair of radii of curvature at their end points. The graph graduations are in millimeters.

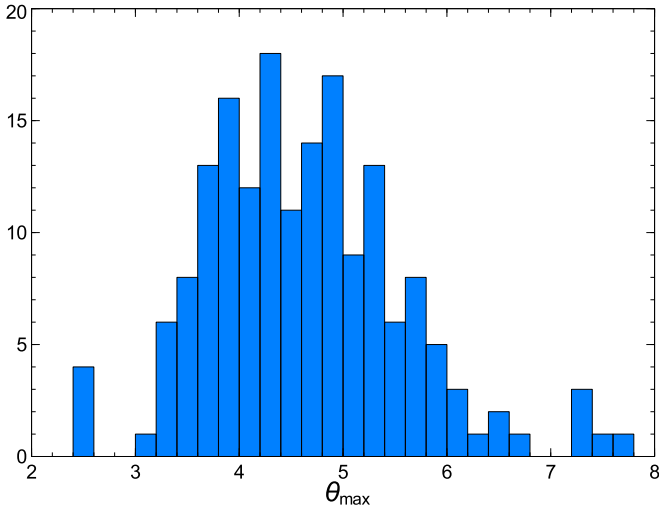

Fig. S7. Distribution of θ_{max} defined as the maximal value of the polar angle of the analyzed spiral segments.

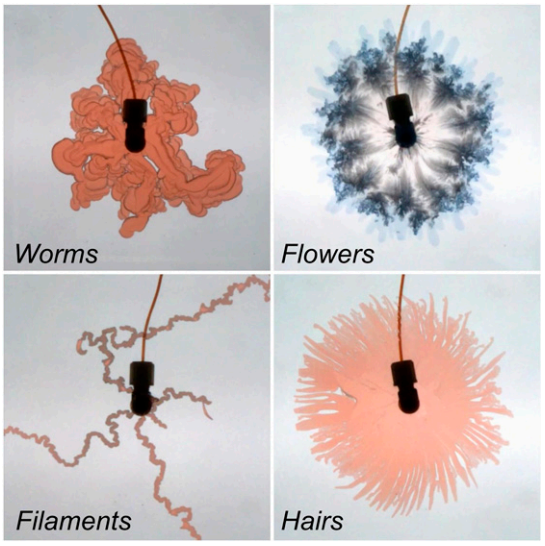

Movie S1. Some examples of chemical gardens growing in a confined geometry upon injecting one solution of cobalt chloride into sodium silicate.

Movie S1

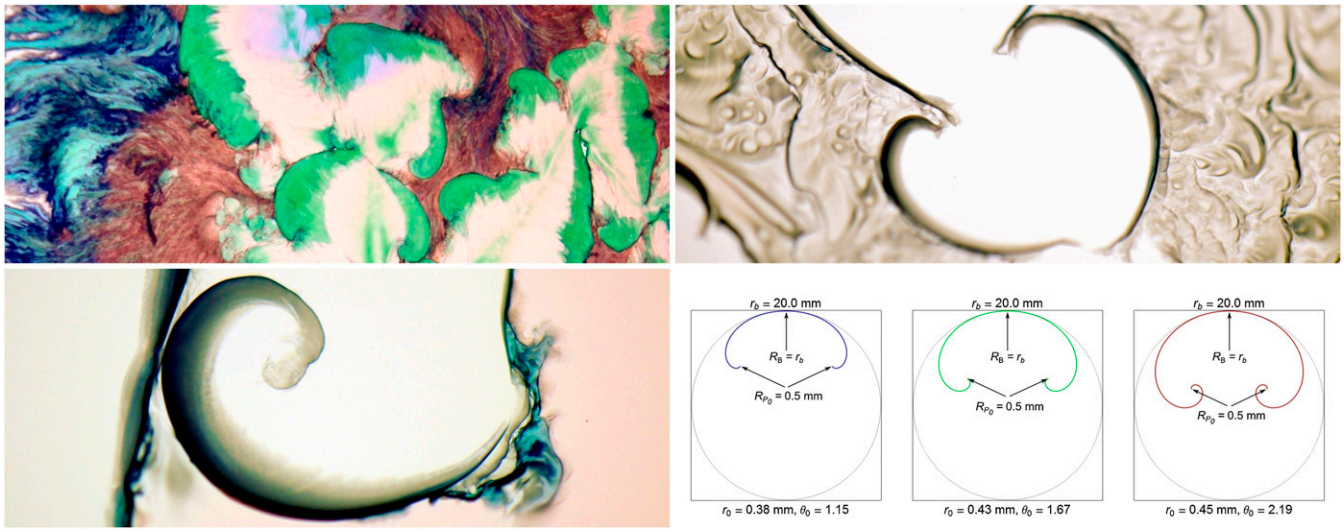

Movie S2. Photos of spiraling precipitates and animation of the spiral growth according to the geometrical model.

Movie S2

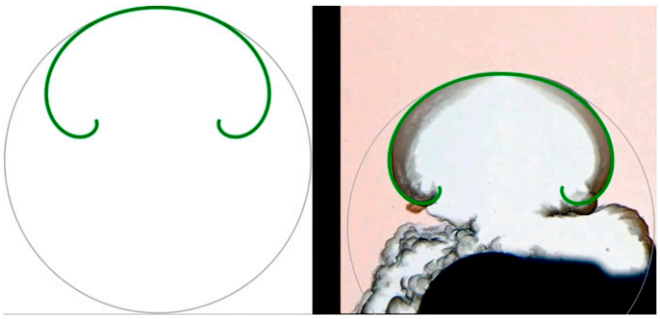

Movie S3. Qualitative comparison between the spiral growth observed in experiments and the one obtained from the geometrical model.

Movie S3